33RD CONGRESS
OF THE INTERNATIONAL COUNCIL
OF THE AERONAUTICAL SCIENCES
STOCKHOLM, SWEDEN, 4–9 SEPTEMBER, 2022

ICAS 2022 SWEDEN

NUMERICAL STUDY ON WATER DISPLACEMENT DRAG CHARACTERISTICS OF AIRCRAFT ELASTIC TIRE ON CONTAMINATED RUNWAYS

Chenhui Ge[1], Peiqing Liu[1], Qiulin Qu[1]

[1]School of Aeronautic Science and Engineering, Beihang University, Beijing 100191, Peoples' Republic of China

Abstract

Modern aircraft is required to have the ability to take off and land safely under complex weather conditions. During the taxiing process of the aircraft on contaminated runways, the impact and extrusion of the tire on the water film would generate a large water displacement drag, which would have a significant influence on the take-off and landing performance of the aircraft. In this study, the Smoothed Particle Hydrodynamics (SPH) and the Finite Element Method (FEM) are applied to numerically simulate the fluid-structure interaction between the tire and water. On the solid side, the FEM is used to deal with elastic deformation of taxiing tire and tire-ground contact. On the fluid side, the SPH method is used for the numerical simulation of water spray generated by aircraft tire. A contact-impact algorithm based on the penalty method is used for the coupling interface between fluid and structure. The reliability and accuracy of the numerical methods are validated by the comparison of tire-generated water spray between the SPH simulation and the experiment test. According to the results, the characteristics of water displacement drag and water spray generated by elastic tire during the taxiing process depend heavily on the translational speed. It is found that, under the conditions of the same forward speed, vertical deflection and water film thickness, the pavement roughness will have a significant influence on the water displacement drag. The blocking effect of the rough pavement on the water flow leads to the increase of the additional drag. Additionally, the effect of tire speed on the spray patterns are analyzed.

Keywords: elastic tire, water displacement drag, SPH, fluid-structure interaction

1. Introduction

A runway is considered contaminated by water when more than 25% of its used surface is covered by standing water more than 3 millimeters (1/8 inch) deep[1-2]. As the moving tire contacts and displaces the stationary runway fluid when an aircraft takes off and lands, the resulting change in momentum of the fluid creates hydrodynamic pressures that react on the runway and tire surfaces. The retardation forces due to hydrodynamic pressures increases the take-off distance required by the airplane and under certain conditions would prevent the airplane from obtaining the required take-off velocity[3]. Furthermore, the deformation and fragmentation of the free surface, under the hydrodynamic pressure, form the forward and lateral spray which will impact the aircraft. The additional drag composed of water displacement drag due to hydrodynamic pressure and impingement drag due to water spray will have a significant influence on the take-off performance of the aircraft. Therefore, it is necessary to study the characteristics of the additional drag.

In the early studies, several flight tests and laboratory experiments were carried out to measure the hydrodynamic forces on aircraft tires and observe the manifestations of tire hydroplaning. Horne et al.[3] conducted a series of unbraked taxi tests at the NASA Langley Research Center to measure the tire retardation forces developed during rolling in both slush and water. The results indicated that with the increase of forward velocity, the water displacement drag increases parabolically, and increases approximately linearly with the increase of water depth. Based on the experimental results, they proposed the estimation equation of the water displacement drag on the unbraked tire. The estimation method of water displacement drag and impingement drag in aircraft airworthiness

assessments is illustrated detailly in ESDU[4] and EASA AMC 25.1591[5]. Giesberts et al.[6-7] conducted the flight tests with a Cessna aircraft on the water-contaminated runway. They calculated the drag caused by the standing water based on the difference in acceleration of the aircraft on the dry and wet runways. The experimental results showed that the measured additional drags for the complete aircraft and the main gear only were significantly higher than the estimated values. Similarly, the test results of Van et al.[8] also had a large deviation from that obtained by the estimation methods. It can be seen that the estimation of additional drag by the empirical formula is not accurate enough. Moreover, it is difficult to accurately distinguish the friction and water displacement drag by experimental method when the tire-pavement contact area changes. Therefore, it is necessary to employ a reliable numerical method to study the dynamics of water displacement drag generated by the tire.

The dynamics of an elastic tire rolling on the water-contaminated runway is a complex problem of fluid-structure interaction. In recent decades, several coupling numerical methods have been developed for simulating the process of the tire impacting water film, such as the Finite Element Method (FEM) with the arbitrary Lagrangian-Eulerian algorithm and coupled Eulerian-Lagrangian algorithm, coupling of FEM and Finite Volume Method (FVM) and coupling of FEM and Smoothed Particle Hydrodynamics method (SPH). The majority of numerical studies are concerned about hydroplaning of tires and variation of tire-pavement friction. That is, the calculation of the vertical forces is the main objective, including the hydrodynamic lift force and the pavement-tire supporting force. Based on the hydrodynamic lift force obtained by simulation, the critical hydroplaning speed can be predicted[9]. The influence of several types of tire patterns[10-13] on hydroplaning behavior also can be analyzed. Furthermore, some researchers studied the skid resistance of the braking tires based on the variation of tire-pavement friction and fluid drag with the tire velocity[14-16]. However, there is still a lack of systematic analysis on the mechanics of water displacement drag generated by the freely rolling tire at various speeds.

The effect of pavement roughness on tire hydroplaning was investigated by several experiments[17] and numerical simulations[18-19]. It is found that the pavement roughness leads to an increase of the fluid loading which are responsible for a loss of contact between the tire and the ground. As the horizontal component of hydrodynamic force, water displacement drag is also affected by the pavement roughness. Therefore, it is necessary to carry out numerical study on the characteristics of water displacement drag under different pavement roughness.

In this paper, the coupling method of SPH and FEM is employed to simulate the process of elastic tire freely rolling on the water-contaminated runway. The hydrodynamic forces generated by the fluid-structure interaction are obtained. Subsequently, the influence of tire forward speed and pavement roughness on water displacement drag is quantitatively analyzed. Furthermore, there are comparisons of spray patterns and water contents at different speeds.

2. Numerical method and physical model

2.1 Coupling method of SPH and FEM

The process of an elastic pneumatic tire moving on the water-contaminated runway is complicated, which involves the large deformation and breakup of water film, the elastic deformation of tire structure, and fluid-structure interaction. In this paper, the SPH method[20-22] is employed to simulate the flow and breakup of water film, whilst FEM[23] is employed for the simulation of elastic tire deformation. A contact-impact algorithm is used in the coupling interface of the fluid and tire structure. All simulations are performed using the LS-DYNA software.

The simulation of large deformation and breakup of the free surface flow will significantly increase the algorithmic complexity and the computational costs of the mesh-based approaches. SPH, as a meshless method, shows obvious advantages in simulating the flow of the water film and the spray generated by a rolling tire on the water-contaminated runway[24-27].

The particles are the computational framework on which the governing equations are resolved. The discrete forms of the continuity equation, momentum conservation equation and energy conservation equation in SPH method based on the particle approximation can be written as:

$$\frac{d\rho_i}{dt} = \rho_i \sum_{j=1}^{N} \frac{m_j}{\rho_j} \left(v_i^\beta - v_j^\beta \right) \cdot \frac{\partial W_{ij}}{\partial x_i^\beta} \tag{1}$$

$$\frac{dv_i^\alpha}{dt} = \sum_{j=1}^{N} m_j \left(\frac{\sigma_i^{\alpha\beta}}{\rho_i^2} + \frac{\sigma_j^{\alpha\beta}}{\rho_j^2} \right) \frac{\partial W_{ij}}{\partial x_i^\beta} \tag{2}$$

$$\frac{dE_i}{dt} = \frac{1}{2} \sum_{j=1}^{N} m_j \left(\frac{p_i}{\rho_i^2} + \frac{p_j}{\rho_j^2} \right) \left(v_i^\beta - v_j^\beta \right) \frac{\partial W_{ij}}{\partial x_i^\beta} + \frac{\mu_i}{2\rho_i} \varepsilon_i^{\alpha\beta} \varepsilon_j^{\alpha\beta} \tag{3}$$

where subscripts i and j are particle identifiers. Superscripts α and β are the space indexes. N is the number of particles in the influence domain of particle i. m, x, ρ, v and E are the mass, location, density, velocity and energy of the particle, respectively. σ is the total stress tensor including the isotropic pressure p and viscous stress tensor τ, μ is the viscosity coefficient and ε is the strain tensor. W is the kernel function.

The classical Finite Element Method is employed for simulating the deformation of elastic tires. In FEM, the consecutive object is divided into a set of units. By solving a set of linear equations, which is achieved from equilibrium conditions, the displacement and stress of each unit and node can be obtained. The common form of basic equations in FEM can be written as:

$$\boldsymbol{M}\ddot{\boldsymbol{U}} + \boldsymbol{C}\dot{\boldsymbol{U}} + \boldsymbol{K}\boldsymbol{U} = \boldsymbol{F} \tag{4}$$

where $\boldsymbol{M}$ is the mass matrix, $\boldsymbol{C}$ is a damping matrix and $\boldsymbol{K}$ is the stiffness matrix. $\boldsymbol{U}$ is the displacement vector of the nodes and $\boldsymbol{F}$ is the load vector. $\ddot{\boldsymbol{U}}$ and $\dot{\boldsymbol{U}}$ denote the nodal accelerations and velocities, respectively.

Furthermore, a contact-impact algorithm based on the standard penalty formulation is employed to resolve the fluid-structure interaction. Interfaces can be defined in three dimensions by listing in arbitrary order all segments that comprise each side of the interface. One side of the interface is designated as the slave side, and the other is designated as the master side. The penalty method consists of placing normal interface springs between all penetrating nodes and the contact surface[28].

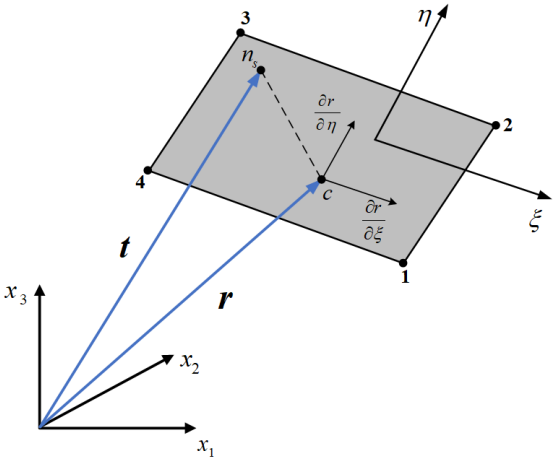

Figure 1 - Location of contact point when the slave node lies above a master segment.

Assume that a master segment has been located for slave node n_s. Then the point nearest to n_s on the master segment is defined as the contact point c, as shown in Figure 1. $\boldsymbol{r}$ and $\boldsymbol{t}$ are the position vectors of c and n_s, respectively. ξ and η are the coordinate system on the master segment. If slave node n_s has penetrated through master segment s_i, an interface force vector $\boldsymbol{f}_s$ will be added which is written as:

$$\boldsymbol{f}_s = -lk_i\boldsymbol{n}_i \tag{5}$$

where l is the penetration length of the slave node, $\boldsymbol{n}_i$ is the unit normal vector of the master segment at the contact point. The stiffness factor k_i for master segment s_i is given in terms of the bulk modulus K_i, the volume V_i and the face area A_i of the brick element that contains s_i as:

$$k_i = \frac{f_{si} K_i A_i^2}{V_i} \tag{6}$$

where f_{si} is a scale factor for the interface stiffness.

2.2 Physical model

In this paper, the elastic pneumatic tire of a certain type of aircraft is used for the simulation. Under uninflated and unloaded conditions, this type of tire has a diameter of 0.511m, a width of 0.1795m, and four longitudinal grooves with a width and depth of approximately 10mm and 8mm, respectively. The inflation pressure is 150psi (1034kPa) and is treated as distributed load applied to the inner surface of the tire. Figure 2 represents the three-dimensional finite element model of the tire.

Figure 2 - Finite element model of the elastic pneumatic tire.

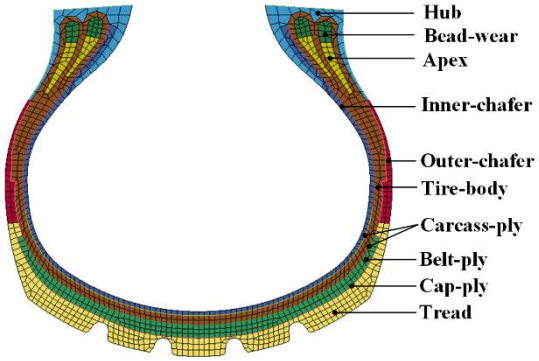

Figure 3 - The profile of finite element tire model.

The elastic tire has a complex structure composed of several materials, as shown in Figure 3. In the numerical simulation, the rubber components are modeled with solid elements. While the reinforcements are modeled with orthotropic shell elements. A layer of rigid shell elements is placed on the outer surface of the hub to be applied the vertical load. The tire mesh contains 736,440 solid elements and 73,800 shell elements, where the minimum cell size is 2.5mm.

The standing water film on the contaminated runway is discretized by SPH particles. As shown in Figure 4, the length and width of the entire water film area are 2.25m and 1m, respectively. The free surface of the water film is defined as the x-y plane in the global coordinate system, and the symmetry plane is defined as the x-z plane. In order to reduce the number of particles involved in the simulation while concentrating the accuracy in the tire-water contact area, the computational domain is divided into three areas. The finest spatial resolution is applied to the Zone I with a length of 1.6m and a width of 0.4m where the tire-water contact occurs. The fluid spatial resolution Δx_{SPH} in Zone I is set to 2mm. While in the Zone II and Zone III where no tire-water contact occurs in the simulation, Δx_{SPH} is set to 3mm and 5mm, respectively.

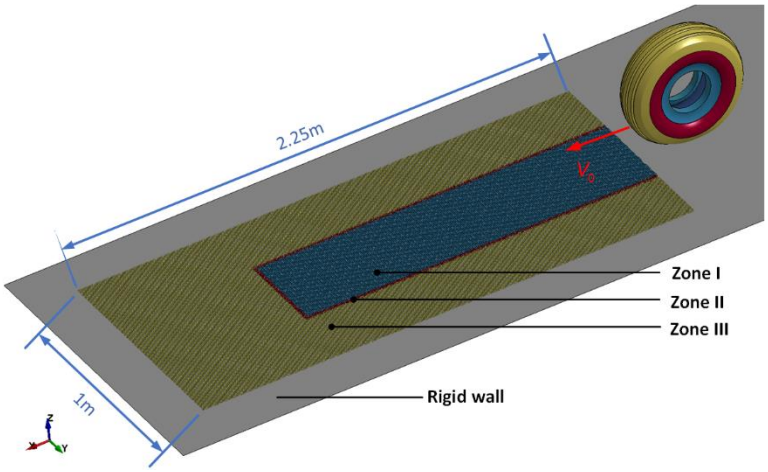

Figure 4 - Computational model of an elastic tire freely rolling on the water-contaminated runway.

The same material properties as water, the density of SPH particles is $1000 kg/m^3$ and the viscosity coefficient is $0.001 kg/m \cdot s$. The Gruneisen equation of state is used, with the parameters shown in Table 1.

Table 1 - Parameters in the Gruneisen equation of state for water

Parameter	$C(m/s)$	S_1	S_2	S_3	γ_0	α
Value	1480	2.56	-1.986	0.2268	0.5	2.67

The runway is considered as a rigid wall since the deformation of the pavement is negligible under the vertical load of the tire. As shown in Figure 4, the runway is modeled by rigid shell elements with no thickness. When the aircraft is taxiing during take-off, the unbraked wheels roll freely under the no-slip contact condition between tire and pavement. Furthermore, it can be basically simulated that the macroscopic influence of pavement roughness on hydrodynamic characteristics, by setting the friction coefficient between pavement elements and SPH particles.

Based on the methods and models presented above, several cases with different tire speeds V_0 and water-pavement friction coefficients μ_f are simulated. It should be noted that the main objective of this paper is to analyze the effect of tire speed and pavement roughness on water displacement drag. Therefore, all cases are carried out under the conditions of the same water film thickness h and tire vertical deflection δ. The parameters of the simulation cases are shown in Table 2.

Table 2 - Parameters of the simulation cases

Case	$V_0(m/s)$	μ_f	h/mm	δ/mm
1	20	0.1	12	30
2	25	0.1	12	30
3	30	0.1	12	30
4	35	0.1	12	30
5	40	0.1	12	30
6	45	0.1	12	30
7	50	0.1	12	30
8	30	0.05	12	30
9	30	0.15	12	30
10	30	0.2	12	30
11	30	0.25	12	30
12	30	0.3	12	30
13	30	0.5	12	30
14	30	0.7	12	30

3. Validation of numerical methods

In our previous studies[24-27], the ability of the SPH method to predict the formation of tire water spray is assessed by simulating the NASA experimental test case[29]. The 6.00 × 6, TT, 8-ply, type III aircraft tire with the initial radius of $r = 0.234m$ and the width of $w = 0.1524m$ is used in the validation. The tire load is 11,120N (2,500lb.), and the inflation pressure is 241,325Pa (35psi). The water depth is $0.0653r$, and the test speed is $24.384\,m/s$. In the test, an array of water collection tubes was used to catch the water for flow rate measurements. Figure 5 presents the comparison of SPH simulation and NASA measurement results. For the major spray region near the tire, the spray angle from the SPH simulation results is very close to that of the NASA test. The effect of airflow on the major spray region is weak where the jet does not completely break up into tiny droplets. However, the airflow, which is neglected in SPH simulation, has a significant effect on the trajectories of the droplets in the region far away from the tire. Thus, there is some discrepancy in the spray angle between the simulation and measurement results in that region.

As aforementioned, this paper focuses primarily on the hydrodynamic force in the main interaction area between the tire and water film, which the influence of airflow can be ignored. Therefore, SPH method is effective and reliable for the simulation of tire-water interaction.

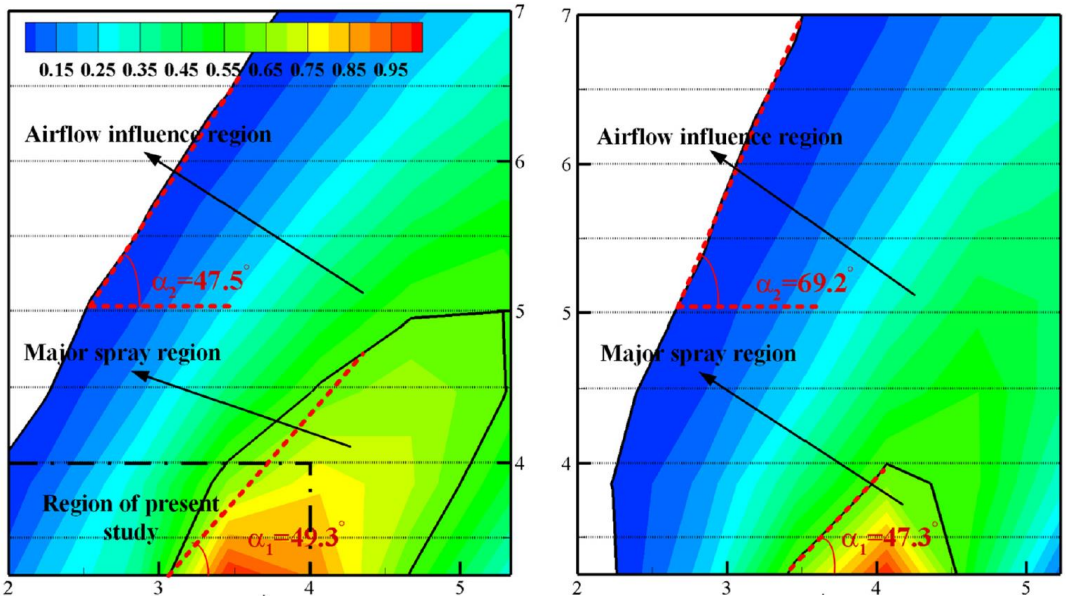

a) SPH result b) NASA measurement

Figure 5 - Comparison of the spray mass density contours between the SPH simulation and the NASA measurement.[27]

4. Results and discussion

4.1 Water displacement drag characteristics under the influence of tire speed

In the process of the tire rolling freely on the water-contaminated runway, the impact and squeezing of the tire on the water film will generate a great hydrodynamic force. By employing the SPH-FEM coupling method, combined with the contact-impact algorithm based on the penalty formulation, the force of SPH particles on the tire elements can be calculated. The horizontal component of the interaction force between SPH particles and elements is the water displacement drag on the rolling tire. Figure 6 presents the time histories of water displacement drag F_w at different tire speeds V_0. The initial contact time between the tire and water film is defined as $t = 0$. Obviously, in the process of the tire entering the water film area at a constant speed, the water displacement drag gradually increases. The drag is basically stable when the tire is in full contact with water. Since the hydrodynamic force is obtained by integrating the interface force vectors between slave nodes and master segments in a certain time step Δt , the calculation results are affected by the spatial resolution of SPH particles. In Figure 6, F_w fluctuates within a small range when the tire moves steadily. However, the focus is on the time-averaged results at different tire speeds in evaluating the effect of F_w on the take-off performance of an aircraft. The small fluctuations in the simulation results are

tolerable.

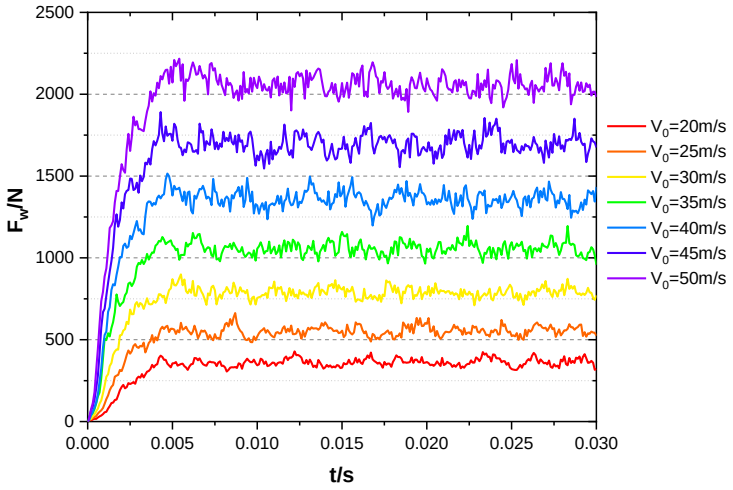

Figure 6 - Variation of water displacement drag with time at different tire speeds.

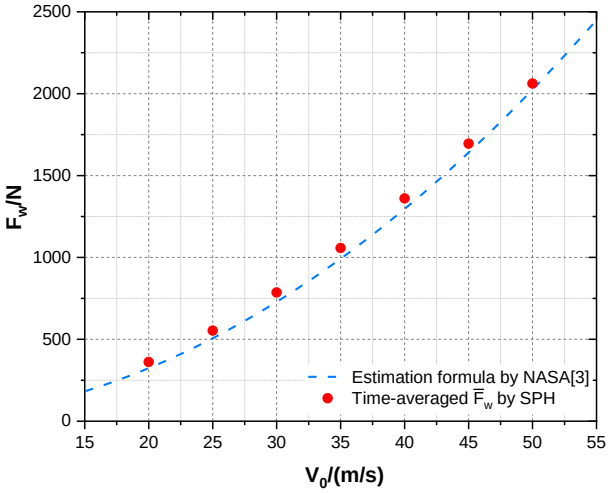

Figure 7 - Comparison of time-averaged $\bar{F}_w$ obtained by SPH (red dots) with the estimation formula proposed by NASA (dash line)[3].

The time-averaged $\bar{F}_w$ can be calculated by the formula as followed:

$$\bar{F}_w = \frac{1}{t_2 - t_1}\int_{t_1}^{t_2} F_w dt \tag{7}$$

where t_1 and t_2 are the start time and end time of time-averaged sampling, respectively. According to Figure 6, it can be set as $t_1 = 0.005s$ and $t_2 = 0.030s$. The red dots in Figure 7 represents the time-averaged $\bar{F}_w$ at different tire speeds. Under the condition of constant water film thickness and tire vertical deflection, the water displacement drag increases significantly with the increase of speed. Horne et al. [3] proposed an estimation formula for F_w based on their experimental results. The water displacement drag is modelled using the analogy with aerodynamic drag and is expressed as:

$$F_w = C_D \frac{1}{2}\rho V_0^2 S \tag{8}$$

where ρ is the density of water, S is the frontal area of the tire. S is defined as $S = bh$ where h is the water film thickness and b is the effective tire width can be written as:

$$b = 2W\left[\left(\frac{\delta+h}{W}\right)-\left(\frac{\delta+h}{W}\right)^2\right]^{\frac{1}{2}} \tag{9}$$

where W is the maximum width of the tire and δ is the tire vertical deflection. The value of C_D is usually taken as 0.75 below the hydroplaning speed.

The simulation results for $\bar{F}_w$ by SPH method are in good agreement with the estimation formula shown by the dash line in Figure 7. It is illustrated that the SPH-FEM coupling method used in this paper is effective and accurate for calculating the hydrodynamic force. Furthermore, this method can be employed for the quantitative analysis of water displacement drag under different tire models and various factors.

4.2 Water spray characteristics at different speeds

A large mass of splashing will be generated in the process of the tire moving on the water-contaminated runway. As the tire moves at a constant speed to a steady state, the spray angle is basically stable. Additionally, the spray patterns are similar at different times, as shown in Figure 8. It can be seen that the water content in the lateral spray accounts for a large part of the total tire-generated spray. Compared with lateral spray, the forward spray caused by bow wave in front of the tire has less water content. According to the formation mechanism, Zhang et al. [27] divided the lateral spray into two separate areas, namely impact-generated side plume near the tire and wave-generated side plume away from the tire. Bow wave and impact-generated side plume are generated by the rolling tire squeezing and impacting the undisturbed water film. Subsequently, the bow wave forms a forward spray with a high horizontal velocity.

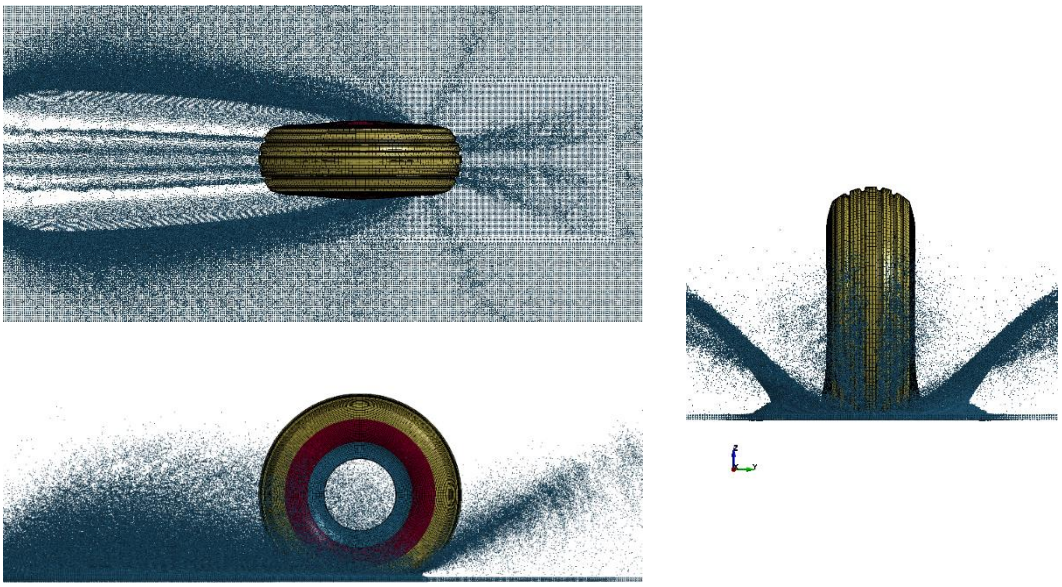

Figure 8 - Water spray generated by the tire moving on water-contaminated runway in Case3.

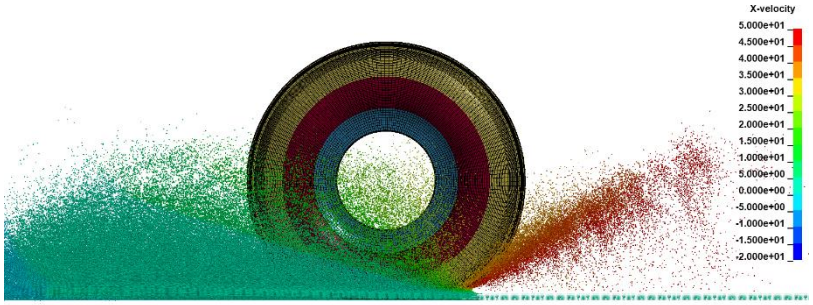

Figure 9 - The distribution of particle horizontal velocity in water spray (Case3).

As shown in Figure 9, the horizontal velocities of SPH particles in bow wave are much higher than that of lateral spray. The horizontal momentum increase of bow wave reacts to the tire and causes a

considerable part of water displacement drag. Bow wave is an accompanying phenomenon in the formation process of water displacement drag. The characteristics of water content and spray angle in bow wave is strongly related to the tire speed.

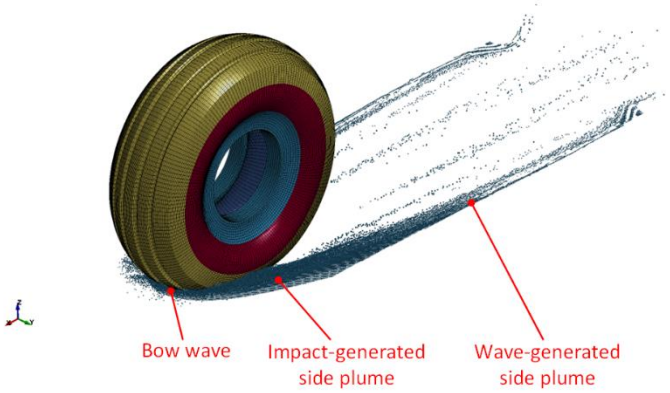

Figure 10 - Distribution of water spray generated in the time period of $\Delta t = 5ms$.

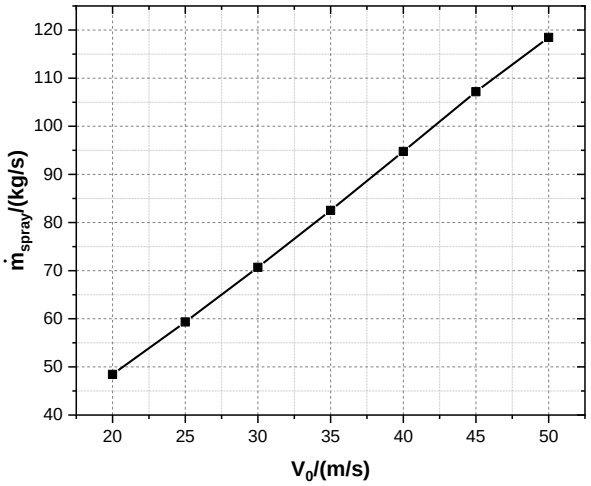

Figure 11 - Spray mass rate of bow wave at different tire speeds.

By counting the number of SPH particles moving into the area above the unperturbed surface level of film, the mass of water spray can be obtained. Figure 10 presents the distribution of water spray generated in the time period of $\Delta t = 5ms$. Bow wave concentrates in front of the tire and contributes to the formation of water displacement drag. While the impact-generated lateral spray mainly contributes to the hydrodynamic lift force. Wave-generated lateral spray has no effect on hydrodynamic force as there is no interaction with the tire. As shown in Figure 11, the spray mass rate of bow wave increases linearly with the tire speed.

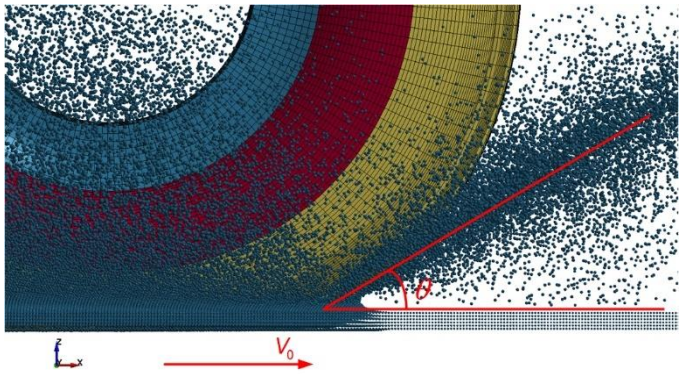

Figure 12 - Angle θ between the bow wave and unperturbed free surface.

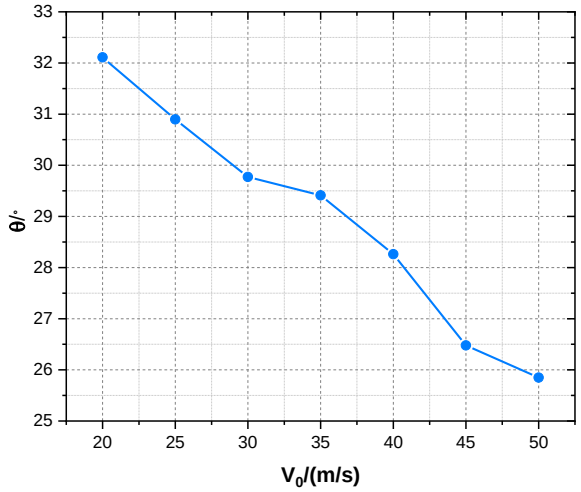

Figure 13 - Variation of forward spray angle θ with the tire speed.

In the simulations, the forward spray angle θ is obtained by fitting the coordinates of SPH particles in the x-z plane with the least square method. As shown in Figure 13, the forward spray angle θ between the bow wave and the unperturbed free surface tends to reduce progressively as the tire speed increases, which is similar to the experimental results of Horne et al. [3]. The horizontal velocity of bow wave increases with the tire speed, while the vertical velocity changes little, resulting in the reduction of forward spray angle.

By using SPH method, the characteristics of water content and spray angle at different speeds can be quantitatively analyzed, which provides a support for the safety assessment of aircraft take-off and landing on the water-contaminated runway.

4.3 The influence of pavement friction on hydrodynamic force

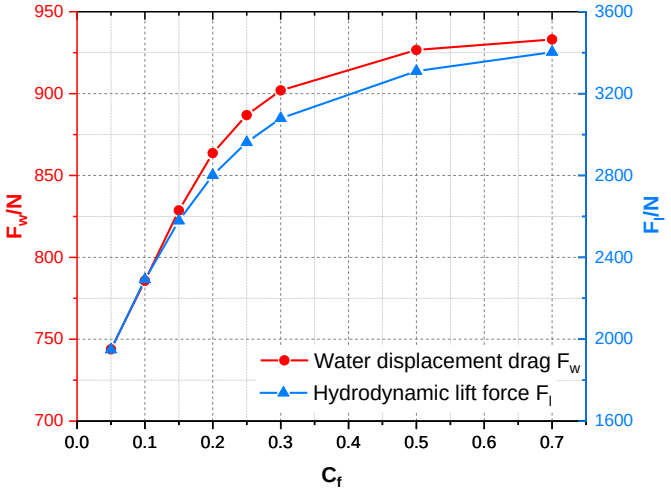

Figure 14 - Variation of water displacement drag F_w (red line) and hydrodynamic lift force F_l (blue line) with the pavement friction coefficient C_f.

In the experiment conducted by Hermange et al. [17], it is illustrated that the pavement roughness leads to an increase of the fluid loading which resulting in a loss of the tire-pavement contact area. By setting different friction coefficients between pavement and water film, the influence of pavement roughness on hydrodynamic force is quantitatively analyzed.

The movement of the SPH particles at the bottom layer in contact with the pavement will be retarded by friction. This can simulate the blocking effect of rough road on water flow. Under the action of friction, the water drainage rate between the tire and pavement decreases, resulting in the increase

of hydrodynamic pressure. The red line and blue line in Figure 14 represent water displacement drag and hydrodynamic lift force, respectively. It is indicated that both the horizontal and vertical components of the hydrodynamic force increase with the friction coefficient. According to the curves in Figure 14, the derivative of hydrodynamic force with respect to friction coefficient, including $\partial F_w/\partial C_f$ and $\partial F_l/\partial C_f$, decreases with the increase of C_f. That is, when the friction coefficient is small, the hydrodynamic force is significantly affected by friction. However, when the friction coefficient is large, the hydrodynamic force converges to a certain constant. It is necessary to introduce the influence of pavement roughness when evaluating the hydrodynamic characteristics of the tire rolling on water-contaminated runway.

5. Conclusions

The coupling method of SPH and FEM is employed for simulating the process of elastic tire freely rolling on the water-contaminated runway. The hydrodynamic forces generated by the fluid-structure are obtained. Under the condition of constant water film thickness and tire vertical deflection, the water displacement drag increases significantly with the increase of speed. By comparing the simulation results and estimation formula, the SPH-FEM coupling method used in this paper shows good effectiveness and accuracy in calculating hydrodynamic forces.

The characteristics of water content and spray angle in bow wave is strongly related to the tire speed. Bow wave concentrates in front of the tire and contributes to the formation of water displacement drag. As the tire speed increases, the spray mass rate of bow wave increases linearly. While the forward spray angle between the bow wave and the unperturbed free surface tends to reduce progressively as the tire speed increases.

The influence of pavement roughness on hydrodynamic forces is quantitatively analyzed. Due to the blocking effect of rough pavement on water flow, both the horizontal and vertical components of the hydrodynamic force increase with the friction coefficient. Furthermore, the hydrodynamic force is significantly affected by the pavement roughness when the friction coefficient is small.

6. Contact Author Email Address

Qiulin Qu: qql@buaa.edu.cn

7. Copyright Statement

References

[1] JAA. *Supplementary Performance Information for Take-Off from Wet Runways and for Operations on Runways Contaminated by Standing Water, Slush, Loose Snow, Compacted Snow or Ice*. JAR-25 AMJ 25X1591, 1993.

[2] FAA. *Water Ingestion Testing for Turbine Powered Airplanes*. FAA AC 20-124, 1985.

[3] Horne W, Joyner U and Leland T. *Studies of the retardation force developed on an aircraft tire rolling in slush or water*. National Aeronautics and Space Administration, 1960.

[4] ESDU. *Frictional and Retarding Forces on Aircraft Tires*. ESDU Data Item 90035, London, 1992.

[5] EASA. Certification Specifications and Acceptable Means of Compliance for Large Aeroplanes. CS-25 Amendment, 2011.

[6] Giesberts M, Gooden J. Precipitation drag of snow and standing water. *ICAS*, 2000.

[7] Giesberts M. *Test and evaluation of precipitation drag on an aircraft caused by snow and standing water on a runway*. National Aerospace Laboratory NLR, 2001.

[8] Van Es G. Braking Capabilities on Flooded Runways: Flight Test Results Obtained with a Business Jet. *AIAA Flight Testing Conference*, p 3651, 2017.

[9] Nazari A, Chen L, and Battaglia F, et al. Prediction of Hydroplaning Potential Using Fully Coupled Finite Element-Computational Fluid Dynamics Tire Models. *Journal of Fluids Engineering*, Vol. 142, No. 10, 2020.

[10] Seta E, Nakajima Y, and Kamegawa T, et al. Hydroplaning analysis by FEM and FVM: effect of tire rolling

and tire pattern on hydroplaning. *Tire Science and Technology*, Vol. 28, No. 3, pp 140-156, 2000.

[11]Cho J, Lee H, and Sohn J, et al. Numerical investigation of hydroplaning characteristics of three-dimensional patterned tire. *European Journal of Mechanics-A/Solids*, Vol. 25, No. 6, pp 914-926, 2006.

[12]Vincent S, Sarthou A, and Caltagirone J, et al. Augmented Lagrangian and penalty methods for the simulation of two-phase flows interacting with moving solids. Application to hydroplaning flows interacting with real tire tread patterns. *Journal of computational physics*, Vol. 230, No. 4, pp 956-983, 2011.

[13]Hermange C, Oger G, and Le Chenadec Y, et al. In-depth analysis of hydroplaning phenomenon accounting for tire wear on smooth ground. *Journal of Fluids and Structures*, Vol. 111, 2022.

[14]Ong G, Fwa T. Wet-pavement hydroplaning risk and skid resistance: modeling. *Journal of Transportation Engineering*, Vol. 133, No. 10, pp 590-598, 2007.

[15]Fwa T, Ong G. Wet-pavement hydroplaning risk and skid resistance: Analysis. *Journal of Transportation Engineering*, Vol 134, No. 5, pp 182-190, 2008.

[16]Cho J, Lee H, and Yoo W. A wet‐road braking distance estimate utilizing the hydroplaning analysis of patterned tire. *International journal for numerical methods in engineering*, Vol. 69, No. 7, pp 1423-1445, 2007.

[17]Hermange C, Todoroff V, and Biesse F, et al. Experimental investigation of the leading parameters influencing the hydroplaning phenomenon. *Vehicle System Dynamics*, pp 1-18, 2021.

[18]Hermange C, Oger G, and Le Chenadec Y, et al. A 3D SPH–FE coupling for FSI problems and its application to tire hydroplaning simulations on rough ground. *Computer Methods in Applied Mechanics and Engineering*, Vol. 355, pp 558-590, 2019.

[19]Zhu X, Pang Y, and Yang J, et al. Numerical analysis of hydroplaning behaviour by using a tire–water-film–runway model. *International Journal of Pavement Engineering*, Vol. 23, No. 3, pp 784-800, 2022.

[20]Gingold R, Monaghan J. Smoothed particle hydrodynamics: theory and application to non-spherical stars. *Monthly notices of the royal astronomical society*, Vol. 181, No. 3, pp 375-389, 1977.

[21]Monaghan J. Particle methods for hydrodynamics. *Computer Physics Reports*, Vol. 3, No. 2, pp 71-124, 1985.

[22]Gingold R, Monaghan J. Kernel estimates as a basis for general particle methods in hydrodynamics. *Journal of Computational Physics*, Vol. 46, No. 3, pp 429-453, 1982.

[23]Bathe K. *Finite element procedures*. Klaus-Jurgen Bathe, 2006.

[24]Qu Q, Zhang F, and Liu P, et al. Numerical simulation of water spray caused by a rolling airplane tire. *Journal of Aircraft*, Vol. 53, No. 1, pp 182-188, 2016.

[25]Qu Q, Liu T, and Liu P, et al. Simulation of Water Spray Generated by Pneumatic Aircraft Tire on Flooded Runway. *Journal of Aircraft*, Vol. 55, No. 4, pp 1700-1708, 2018.

[26]Zhao K, Liu P, and Qu Q, et al. Flow physics and chine control of the water spray generated by an aircraft rigid tire rolling on contaminated runways. *Aerospace Science and Technology*, Vol. 72, pp 49-62, 2018.

[27]Zhang Y, Liu P, and Qu Q, et al. Characteristics and model of the initial spray caused by an aircraft elastic tire rolling on the water-contaminated runway. *Aerospace Science and Technology*, Vol. 79, pp 610-624, 2018.

[28]Hallquist J, Goudreau G, and Benson D. Sliding interfaces with contact-impact in large-scale Lagrangian computations. *Computer methods in applied mechanics and engineering*, Vol. 51, No. 1-3, pp 107-137, 1985.

[29]Robert H, Sandy M. *Measurements of flow rate and trajectory of aircraft tire-generated water spray*. NASA Technical Report, 1987.